JACS
JOURNAL OF THE AMERICAN CHEMICAL SOCIETY

Article

pubs.acs.org/JACS

meso–*meso* Linked Porphyrin–[26]Hexaphyrin–Porphyrin Hybrid Arrays and Their Triply Linked Tapes Exhibiting Strong Absorption Bands in the NIR Region

Hirotaka Mori,[†] Takayuki Tanaka,[†] Sangsu Lee,[‡] Jong Min Lim,[‡] Dongho Kim,*[,‡] and Atsuhiro Osuka*[,†]

[†]Department of Chemistry, Graduate School of Science, Kyoto University, Sakyo-ku, Kyoto 606-8502, Japan

[‡]Spectroscopy Laboratory for Functional π-Electronic Systems and Department of Chemistry, Yonsei University, Seoul 120-749, Korea

Supporting Information

ABSTRACT: We describe the synthesis and characterization of directly *meso*–*meso* linked porphyrin–[26]hexaphyrin–porphyrin hybrid oligomers and their triply linked (completely fused) hybrid tapes. *meso*–*meso* Linked Ni(II) porphyrin–[26]hexaphyrin–Ni(II) porphyrin trimers were prepared by methanesulfonic acid-catalyzed cross-condensation of *meso*-formyl Ni(II) porphyrins with a 5,10-diaryltripyrrane followed by oxidation with 2,3-dichloro-5,6-dicyano-1,4-benzoquinone (DDQ). The Ni(II) porphyrin moieties were converted to Zn(II) porphyrins via an indirect route involving reduction of the [26]hexaphyrin to its 28π congener, acid-induced denickelation, oxidation of the [28]hexaphyrin, and finally Zn(II) ion insertion. Over the course of these transformations, porphyrin–[28]hexaphyrin–porphyrin trimers have been revealed to take on a Möbius aromatic twisted structure for the [28]hexaphyrin segment. Oxidation of *meso*–*meso* linked hybrid trimer bearing 5,15-diaryl Zn(II) porphyrins with DDQ/$Sc(OTf)_3$ under mild conditions resulted in *meso*–*meso* coupling oligomerization, affording the corresponding dimeric (hexamer), trimeric (nonamer), and tetrameric (dodecamer) oligomers. On the other hand, oxidation of a *meso*–*meso* linked hybrid trimer bearing 5,10,15-triaryl Zn(II) porphyrin terminals with DDQ/$Sc(OTf)_3$ under harsher conditions afforded a *meso*–*meso*, *β*–*β*, *β*–*β* triply linked hybrid porphyrin tape, which displays a sharp and intense absorption band at 1912 nm. Comparison of this extremely red-shifted absorption band with those of Zn(II) porphyrin tapes suggests that the bathochromic-shifting capability of a [26]hexaphyrin unit is large, almost equivalent to that of four individual Zn(II) porphyrin units. As demonstrated, the fusion of porphyrins to [26]hexaphyrin offers an efficient means to expand their conjugation networks, significantly expanding the capabilities attainable for these chromophores.

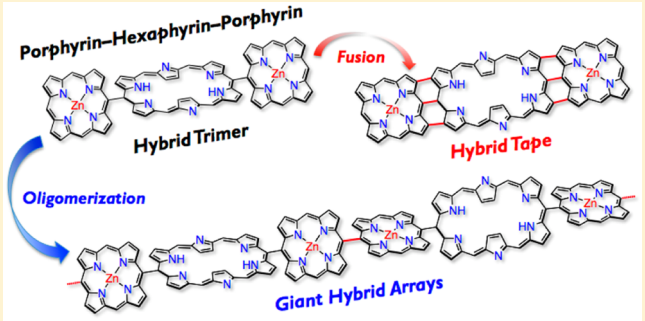

INTRODUCTION

Exploration of highly conjugated porphyrins is one of the hot current topics in porphyrin chemistry, since such molecules are promising candidates for organic conducting materials, near-infrared absorbing dyes, molecular wires, and nonlinear optical materials.[1−3] One such promising subfamily of conjugated porphyrins, namely, *meso*–*meso*, *β*–*β*, *β*–*β* triply linked Zn(II) porphyrin arrays **1**-***n***, so-called porphyrin tapes, show vast potential in light of their fully conjugated π-electronic networks, exceptionally red-shifted absorption bands, and large two-photon absorption (TPA) cross sections (Figure 1).[4−6] In recent years, variants of porphyrin tapes have also been explored, including two-dimensionally extended porphyrin sheets,[7] donor–acceptor type and electron deficient tapes,[8] C_{60}-appended tapes,[9] face-to-face dimeric tapes,[10] and amphiphilic columnar-liquid-crystal forming tapes.[11] While these examples demonstrated a wide range of potential applications of the porphyrin tapes, they tend to become increasingly unstable upon increasing in the number of porphyrin units, since the HOMO levels are increasingly elevated. In addition, longer porphyrin tapes often suffer from serious aggregation, which makes their synthetic manipulations tedious due to poor solubility. Therefore, harmonizing chemical stability and sufficient solubility of conjugated porphyrin tapes that display NIR absorption bands is an essential step for versatile implementation of such molecules.

To this end, we considered structural fusion of porphyrin and [26]hexaphyrin segments, since [26]hexaphyrin **3** is an aromatic molecule possessing a lower-lying S_1 state (ca. 1.2 eV)[12] and has a rectangular conformation whose short side matches well geometrically to the side of a porphyrin. In addition, its electron deficient nature will contribute certain chemical stability to the resulting hybrid tapes by lowering the HOMO level. Along with this line, we previously explored a 1:1 Ni(II) porphyrin–[26]hexaphyrin hybrid tape **4**,[13] and

Received: December 23, 2014
Published: January 22, 2015

DOI: 10.1021/ja5130034
J. Am. Chem. Soc. 2015, 137, 2097−2106

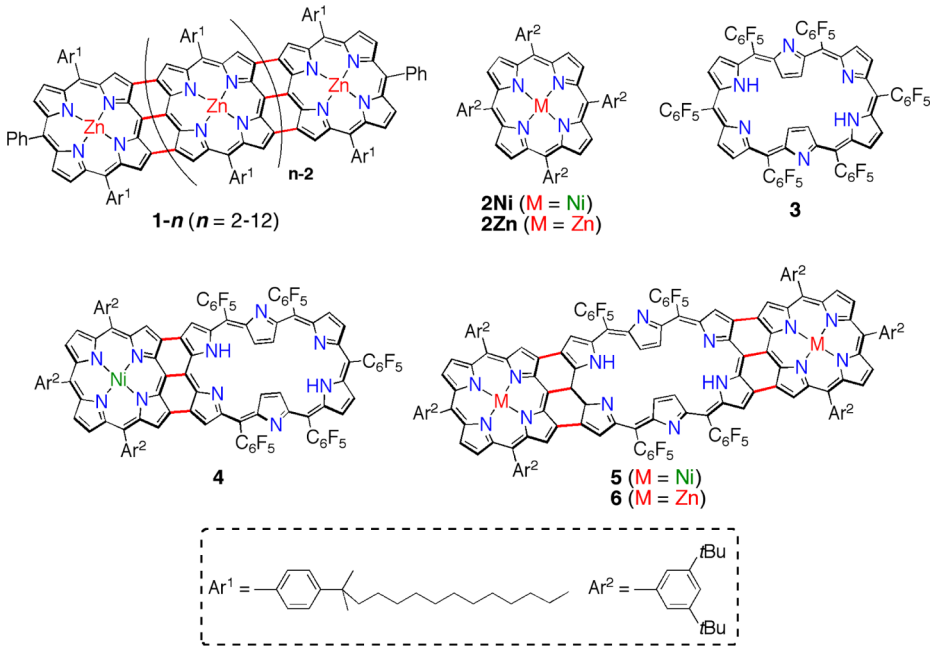

Figure 1. *meso*–*meso*, *β*–*β*, *β*–*β* triply linked porphyrin arrays and fused hexaphyrins.

demonstrated that the fusion of these two porphyrinoids led to a hybrid tape that exhibited an absorption band peaking at 1333 nm, whose intensity was only modest due to its nonsymmetric structure. In this paper, we report the synthesis and characterization of directly *meso*–*meso* linked porphyrin–[26]hexaphyrin–porphyrin hybrid oligomers. These molecules are attractive on their own and important as precursors for the corresponding *meso*–*meso*, *β*–*β*, *β*–*β* triply linked hybrid tapes. Indeed, we succeeded in the synthesis of porphyrin–[26]-hexaphyrin–porphyrin hybrid tapes **5** and **6** via oxidation of *meso*–*meso* linked hybrid trimers, which are reasonably stable under ambient conditions and soluble in common organic solvents. In addition, the NIR absorption of **6** is remarkably red-shifted and intense (λ_{max} = 1912 nm and $\varepsilon = 1.3 \times 10^5$ M^{-1} cm^{-1}).

RESULTS AND DISCUSSION

Preparation of *meso*–*meso* Linked Porphyrin–Hexaphyrin–Porphyrin Hybrid Arrays. *meso*–*meso* Linked Ni(II) porphyrin–[26]hexaphyrin–Ni(II) porphyrin hybrid trimers **9** and **11** were chosen as the first target molecules. Ni(II) porphyrins are robust enough to survive the acidic conditions associated with standard hexaphyrin synthesis. First, we attempted to prepare trimer **9** by using a synthetic method previously developed for the preparation of a *meso*–*meso* linked Ni(II) porphyrin–[26]hexaphyrin dyad.[13] A 33 mM solution of *meso*-formyl Ni(II) porphyrin **7** and 5,15-bis-(pentafluorophenyl)tripyrrane **8** was treated with $BF_3{\cdot}OEt_2$, which, however, did not produce any trace of **9**. Then, we examined a synthetic protocol of A_2B_4-type hexaphyrins,[14] of which the major alterations include the use of methanesulfonic acid instead of $BF_3{\cdot}OEt_2$ and the utilization of a relatively dilute solution of both substrates. After extensive screening, we found reliable synthetic conditions that allowed the synthesis of **9** in 16% yield from the condensation of **7** with **8** (Scheme 1). Under similar conditions, hybrid trimer **11** was prepared from the reaction of **10** with **8** in 28% yield.

Scheme 1. Synthesis of Ni(II) Porphyrin–[26]Hexaphyrin–Ni(II) Porphyrin Hybrid Trimers 9 and 11[a]

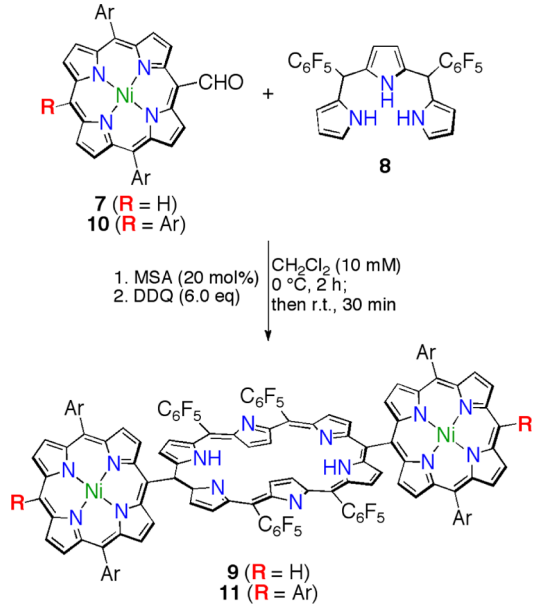

[a]Ar = 3,5-di-*tert*-butylphenyl.

The ^{1}H NMR spectrum of **9** revealed its symmetric structure, exhibiting four doublets due to the *β* protons of the porphyrins and two doublets due to the outer *β* protons of the [26]hexaphyrin moiety in the range 9.30–8.23 ppm, and a singlet due to the *meso*-proton at 10.07 ppm. The inner NH protons and pyrrolic-*β* protons of the hexaphyrin moiety were observed, respectively, as a broad signal at around −1.80 ppm and a singlet at −2.33 ppm (see the Supporting Information). These ^{1}H NMR spectral features indicate that the Ni(II) porphyrin segments are connected at the short sides of the rectangular [26]hexaphyrin framework. The structure of **9** has actually been revealed by X-ray diffraction analysis, as depicted

DOI: 10.1021/ja5130034
J. Am. Chem. Soc. 2015, 137, 2097–2106

in Figure 2a.[15] In this molecular structure, the Ni(II) porphyrins take on considerably ruffled structures and are

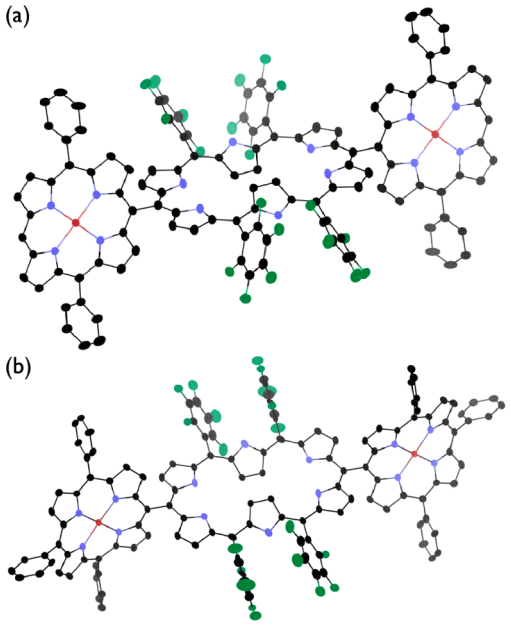

Figure 2. X-ray crystal structures of **9** (a) and **11** (b). Solvent molecules, *tert*-butyl groups of *meso*-aryl substituents, and all hydrogen atoms are omitted for clarity. The thermal ellipsoids are scaled to 30% probability level.

tilted by ca. 82° toward the central mean plane of the [26]hexaphyrin segment. The absorption spectrum of **9** showed a Soret band at 408 nm for the Ni(II) porphyrin units and a Soret-like band at 571 nm and Q-like bands at 751, 903, and 1032 nm for the [26]hexaphyrin unit, all of which are observed at nearly the same positions of the corresponding reference molecules **2Ni** and **3** (Figure 3a). These absorption features of **9** suggest only small electronic interaction exists between the constituent porphyrinoids in spite of the direct connection, which has been ascribed to the almost orthogonal relationship of the Ni(II) porphyrin units toward the [26]hexaphyrin framework. In a similar manner, trimer **11** exhibits ^{1}H NMR and absorption spectra that are analogous to those of **9**, except for the presence of the terminal *meso*-aryl substituents (Supporting Information). The structure of **11** was also determined by X-ray diffraction analysis. In the molecular structure of **11**, the Ni(II) porphyrin segments are more ruffled as compared with **9**, and are tilted by ca. 77° to the hexaphyrin segment (Figure 2b).[16]

Zn(II) porphyrin−[26]hexaphyrin−Zn(II) porphyrin trimers **16** and **17** are apparently more suitable substrates for the oxidative oligomerization and fusion reaction because the Zn(II) porphyrin units are much easier to oxidize. We thus attempted the conversions of **9** to **16** and of **11** to **17**. These conversions were initially attempted by direct denickelation of **9** and **11** under acidic conditions. However, these attempts gave only intractable complex mixtures. These failures were ascribed to the intrinsic instability of the [26]hexaphyrin moiety under acidic conditions. Therefore, we took an indirect route via [28]hexaphyrins **12** and **13**. Namely, the reductions of **9** to **12** and of **11** to **13** were accomplished quantitatively with an excess amount of $NaBH_4$ in CH_2Cl_2/MeOH. We also confirmed that oxidations of **12** and **13** with MnO_2 regenerated

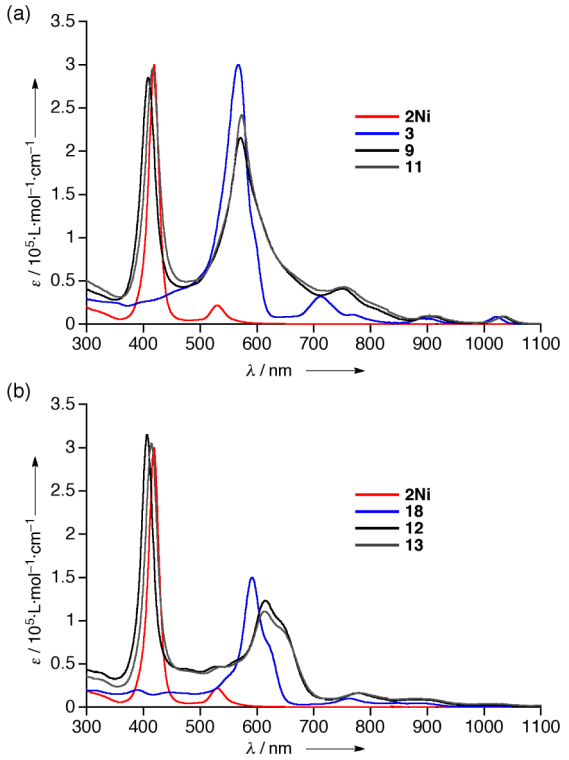

Figure 3. UV/vis/NIR absorption spectra of **9**, **11**, **12**, and **13** and normalized absorption spectra of reference compounds **2Ni**, **3**, and **18** in CH_2Cl_2.

9 and **11**, respectively, with almost quantitative yields (Scheme 2).

Scheme 2. Redox Interconversions between 9 and 11 and 12 and 13 and Preparations of 16 and 17[a]

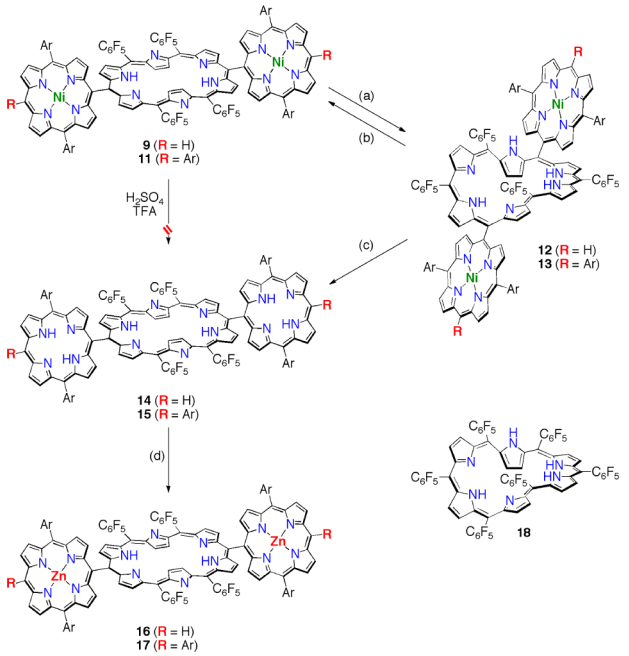

[a](a) $NaBH_4$, CH_2Cl_2/ MeOH, 1 h. (b) MnO_2, CH_2Cl_2, 20 min. (c) H_2SO_4, TFA, 0 °C, then MnO_2, CH_2Cl_2, 20 min. (d) $Zn(OAc)_2 \cdot 2H_2O$, CH_2Cl_2/MeOH, 1 h (Ar = 3,5-di-*tert*-butylphenyl).

DOI: 10.1021/ja5130034
J. Am. Chem. Soc. 2015, 137, 2097−2106

Curiously, the ^{1}H NMR spectrum of [28]hexaphyrin **12** was broad at room temperature but became well-defined at 60 °C, displaying a simple set of sharp signals that seem to portray a rectangular shape in an averaged sense with a moderate diatropic ring current. These spectral features are quite similar to those of hexakis(pentafluorophenyl) [28]hexaphyrin **18**. Therefore, these ^{1}H NMR data can be interpreted in terms of fast conformational dynamics among twisted Möbius aromatic conformers and a rectangular Hückel antiaromatic conformer, as observed for **18**.[17] In line with this interpretation, the ^{1}H NMR of **12** taken at −60 °C showed several sharp signals due to the predominance of Möbius aromatic conformers differing in the special relationship of the two Ni(II) porphyrins (Scheme S1, Supporting Information). The absorption spectrum of **12** exhibited a sharp Soret-like band due to the porphyrin chromophores at 407 nm, a broad but distinct Soret-like band at 617 nm, and weak Q-like bands at 777 and 880 nm with a tail reaching to the range 900−1100 nm for the [28]hexaphyrin chromophore (Figure 3b). These absorption features have also indicated that the central [28]hexaphyrin segment takes twisted Möbius conformations predominantly in solution.

Fortunately, crystals of **12** suitable for X-ray diffraction analysis were obtained by slow diffusion of methanol vapor into its solution in 1,2-dichloroethane. In the crystal, the central [28]hexaphyrin segment indeed takes a singly twisted Möbius conformation, as shown in Figure 4.[18] The Ni(II) porphyrin

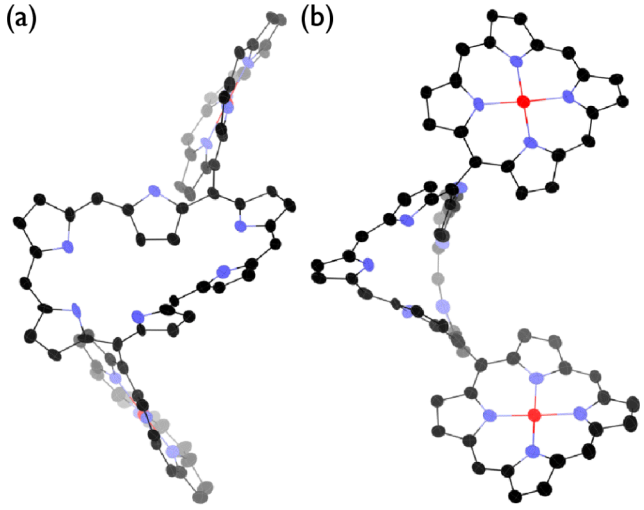

Figure 4. X-ray crystal structure of **12**. (a) Perspective view and (b) side view. Solvent molecules, pentafluorophenyl groups, 3,5-di-*tert*-butylphenyl groups, and all the hydrogen atoms are omitted for clarity. The thermal ellipsoids are scaled at 20% probability level.

units are connected to the twisted [28]hexaphyrin macrocycle at the 5- and 20-positions with dihedral angles of 62 and 63° toward the dipyrromethene segments, respectively, suggesting that small electronic interactions exist between the Ni(II) porphyrin and [28]hexaphyrin segments. Hybrid trimer **13** showed ^{1}H NMR and absorption spectral features that are quite similar to those of **12**, also indicating a Möbius aromatic nature for the central [28]hexaphyrin (Figure S6, Supporting Information).

Transformations of **12** and **13** to **16** and **17** are rather straightforward (Scheme 2). Trimers **12** and **13** were treated with solutions of H_2SO_4 in trifluoroacetic acid to remove the Ni(II) ions and were subsequently oxidized with MnO_2 to furnish **14** and **15** in 93 and 81% yields over the two steps, respectively. The final zincation steps of **14** and **15** required delicate care to avoid over-zincation[19] of the hexaphyrin unit. Therefore, solutions of **14** and **15** in dichloromethane and methanol were treated with 20 equiv of $Zn(OAc)_2{\cdot}2H_2O$ at room temperature for 1 h. Usual aqueous workup gave **16** and **17** in 70 and 93% yields, respectively. Hybrid arrays **14**, **15**, **16**, and **17** were fully characterized by an array of spectroscopic methods (for details, see the Supporting Information). In addition, the structure of **16** has been confirmed by X-ray diffraction analysis (Figure S40, Supporting Information).

Oxidative Homocoupling of Hybrid Trimer. Then, we examined oxidative *meso*−*meso* coupling of **16**. As an initial attempt, a solution of **16** in CH_2Cl_2 was treated with $AgPF_6$ at room temperature followed by elevated temperatures, which were standard conditions for the *meso*−*meso* coupling of 5,15-diaryl Zn(II) porphyrins.[20] However, **16** was recovered almost quantitatively on each occasion. The observed much reduced coupling reactivity of **16** toward $AgPF_6$ as compared with 5,15-diaryl Zn(II) porphyrins has been ascribed to the directly linked electron-withdrawing [26]hexaphyrin. We thus attempted a combined use of $AgPF_6$ and I_2 as a stronger oxidant to accomplish the oxidative *meso*−*meso* coupling. Unfortunately, these hasher conditions resulted in decomposition of **16**. Hypervalent iodine compounds $PhI(OAc)_2$ (PIDA) and $PhI(OCOCF_3)_2$ (PIFA) have been recently reported to be effective reagents for the *meso*−*meso* coupling of Zn(II) porphyrins.[21] These hypervalent iodine compounds have also been examined for the oxidative coupling of **16**. However, PIDA showed no reactivity toward any changes of **16** and PIFA caused decomposition of **16**. Combination of DDQ and $Sc(OTf)_3$, which has been effectively used for the complete fusion reaction of *meso*−*meso* linked Zn(II) porphyrin arrays to *meso*−*meso*, *β*−*β*, *β*−*β* porphyrin tapes,[4,22] was attempted for the oxidative coupling of **16**. When **16** was heated at 80 °C in the presence of 4 equiv of DDQ and $Sc(OTf)_3$, oligomerization of **16** actually proceeded but concomitant fusion reactions were cumbersome, leading to complicated reaction products. After extensive screening of alternative reaction conditions, we found that the oxidation of **16** proceeded selectively with 2 equiv of DDQ and $Sc(OTf)_3$ at room temperature for 2 h, giving hybrid hexamer **16-2** and nonamer **16-3** in 13 and 5% yields, respectively, along with the recovery of **16** (43%). These hybrid arrays were separated by recycling GPC-HPLC (Figure S39, Supporting Information). In this reaction, a small amount of tetrameric trimer (dodecamer) **16-4** was also detected by MALDI-TOF MS and GPC-HPLC analysis of the crude reaction mixture. A separate oligomerization of hexamer **16-2** was attempted under similar conditions to furnish dodecamer **16-4** in 11% yield along with the recovery of **16-2** (48%) (Scheme 3).

The ^{1}H NMR spectra of **16-*n*** (***n*** = **2**−**4**) showed a characteristic singlet due to the terminal *meso*-positions around 10.5 ppm along with doublets due to the outer *β*-H in the range 10−8 ppm, clearly indicating extended linear conformations, as shown in Scheme 3. The parent ion peaks were detected by MALDI-TOF-MS at m/z = 5248 ($[M]^+$; calcd for $C_{300}H_{230}F_{40}N_{28}Zn_4$: 5247) for **16-2**, m/z = 7869 ($[M]^+$; calcd for $C_{450}H_{344}F_{60}N_{42}Zn_6$: 7871) for **16-3**, and m/z = 10499 ($[M]^+$; calcd for $C_{600}H_{458}F_{80}N_{56}Zn_8$: 10495) for **16-4**. The absorption spectra of **16-*n*** (***n*** = **2**−**4**) showed a Soret band of monomeric Zn(II) porphyrin at 415 nm and a split Soret band

DOI: 10.1021/ja5130034
J. Am. Chem. Soc. 2015, 137, 2097−2106

Scheme 3. Oxidative *meso*−*meso* Coupling of 16[a]

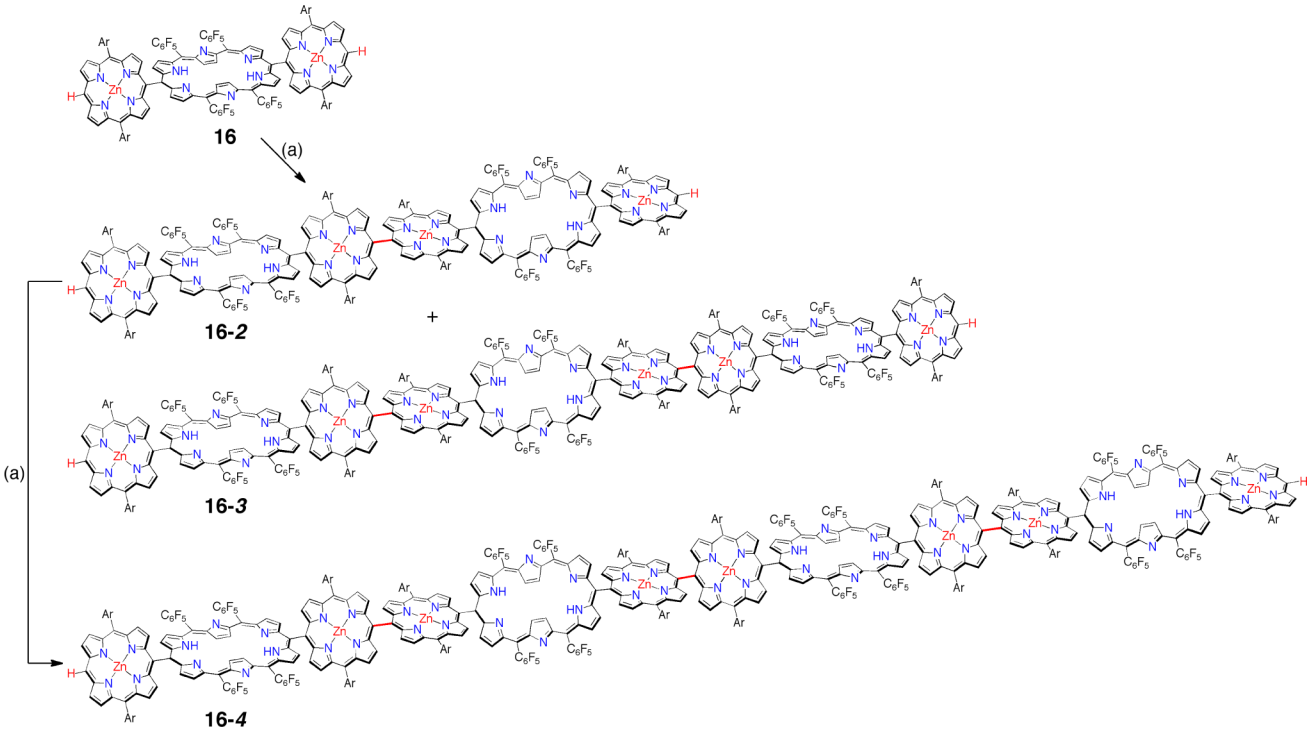

[a](a) DDQ (2.0 equiv), $Sc(OTf)_3$ (2.0 equiv), toluene (3.0 mM), room temperature, 2 h.

of *meso*−*meso* linked Zn(II) diporphyrin at around 416 and 453 nm (Figure 5). The ratio of the former and latter bands

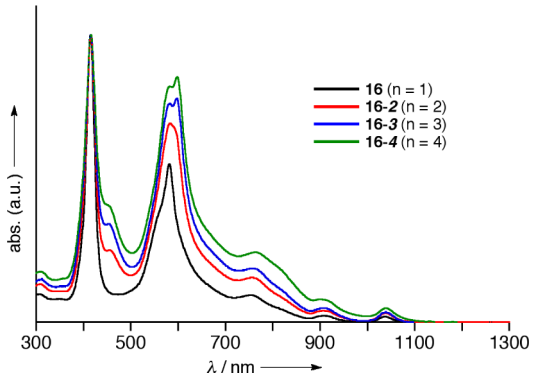

Figure 5. UV/vis/NIR absorption spectra of **16-*n*** in CH_2Cl_2.

increased with an increase in value of ***n***. The Soret-like bands of **16** and **16-2** were observed as a single peak at 582 and 583 nm, but those of **16-3** and **16-4** were observed as two peaks at 582 and 598 nm. The red-shifted Soret-like bands have been assigned due to [26]hexaphyrins bearing two *meso*−*meso* linked Zn(II) diporphyrins, which are found only for **16-3** and **16-4**. Collectively, these absorption spectral features of **16-*n*** are consistent with linearly linked oligomeric structures, as shown in Scheme 3.

Oxidative Fusion of Hybrid Trimers. Next, we examined the oxidative fusion reaction of **11** and **17** (Scheme 4). By following the general method outlined for the synthesis of porphyrin tape derivatives,[4] oxidation of **11** and **17** with DDQ/$Sc(OTf)_3$ in toluene at 80 °C gave *meso*−*meso*, *β*−*β*, *β*−*β*, triply fused hybrid arrays **5** and **6** in 43 and 55% yields, respectively. Both hybrid tapes are reasonably stable under ambient

Scheme 4. Synthesis of Hybrid Tapes 5 and 6[a]

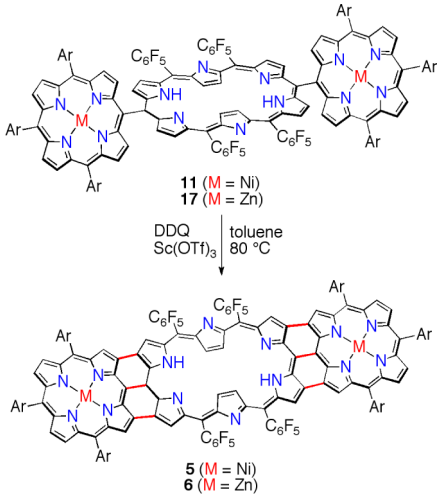

[a]Ar = 3,5-di-*tert*-butylphenyl.

conditions and show good solubilities in common organic solvents.

The ^{1}H NMR spectrum of **5** showed two doublets due to the outer *β*-protons of the terminal porphyrin units at 7.30 and 7.25 ppm, two singlets due to the bay-area protons at 7.24 and 7.15 ppm, a broad signal due to the inner NH protons of the hexaphyrin core at 3.66 ppm, and one singlet due to the inner *β* protons at 2.92 ppm, indicating that a weak diatropic ring current still remains at the central hexaphyrin core. Similar to the ^{1}H NMR spectrum of **5**, that of **6** exhibited four signals due to the peripheral *β* protons in the range 7.13−6.88 ppm and signals due to the inner *β* and NH protons at 4.70 and 5.52 ppm, respectively. Generally, fused porphyrins exhibit a

DOI: 10.1021/ja5130034
J. Am. Chem. Soc. 2015, 137, 2097−2106

comparatively reduced diatropic ring current. Figure S16 (Supporting Information) summarizes the chemical shifts of reference compounds **2Ni**, **2Zn**, **3**, and dimeric and trimeric porphyrin tapes **19** and **20**.[8a] While the signals due to the outer β protons of Ni(II) and Zn(II) tetraarylporphyrins **2Ni** and **2Zn** appear at 8.87 and 9.00 ppm, the ^{1}H NMR spectrum of dimeric porphyrin tape **19** exhibits signals due to the peripheral protons in the range 7.75−7.35 ppm. In a similar fashion, the ^{1}H NMR spectrum of **4** indicates a decreased diatropic ring current, featuring signals due to the peripheral protons of the Ni(II) porphyrin unit in the range 7.17−7.08 ppm and signals due to the outer β protons of the hexaphyrin core in the range 8.56−7.69 ppm, respectively. Characteristically, signals due to the inner β protons of the hexaphyrin core appear at 0.52 and 0.45 ppm, which are downfield-shifted by ca. 3 ppm as compared with those of hexaphyrin **3** (−2.43 ppm). These chemical shifts of the inner β protons can be benchmark values to compare the strength of the diatropic ring current of the hexaphyrin core. According to their chemical shifts, the local aromaticity on the fused hexaphyrin macrocycle of these hybrid tapes can be ordered as follows: **3** (−2.43 ppm) > **4** (0.52 and 0.45 ppm) > **5** (2.92 ppm) > **6** (4.70 ppm) (Figure S16, Supporting Information).

Fortunately, crystals of **6** suitable for X-ray diffraction analysis were obtained from slow diffusion of methanol vapor into its chlorobenzene solution. Figure 6 shows the solid-state

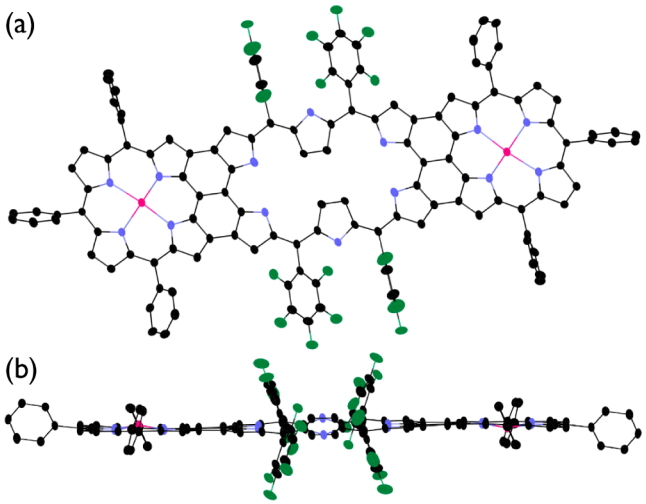

Figure 6. X-ray crystal structure of **6**. (a) Perspective view and (b) side view. Solvent molecules, *tert*-butyl groups of *meso*-aryl groups, and hydrogen atoms are omitted for clarity. The thermal ellipsoids are scaled to 30% probability level.

structure of **6**, in which the porphyrin and hexaphyrin moieties take on fairly planar structures and are held coplanar to each other with a small mean plane deviation (0.08 Å). This coplanar structure is favorable for overall π-conjugation. The $C_{meso}-C_{meso}$ and two $C_\beta-C_\beta$ bond lengths were 1.472, 1.437, and 1.454 Å, respectively.[23] To the best of our knowledge, this is the largest crystal structure of porphyrin tape derivative reported to date.

The UV/vis/NIR absorption spectrum of **5** displays strong absorption in the range 400−1200 nm and a significantly red-shifted Q-like band at 1657 nm (Figure 7). The absorption spectrum of **6** taken in CH_2Cl_2 containing 1% pyridine is similar to that of **5**, but its Q-like band is more red-shifted to

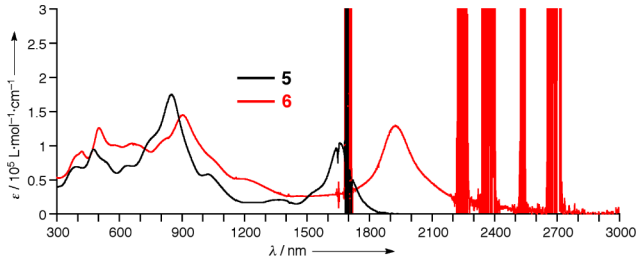

Figure 7. UV/vis/NIR absorption spectra of **5** (black) in CH_2Cl_2 and **6** (red) in CH_2Cl_2 with 1% pyridine.

1912 nm with a full width at half-maximum of 490 cm^{-1} with the absorption tail reaching out to around 2600 nm. This low-energy but sharp absorption band of **6**, when compared with those of Zn(II) porphyrin tapes **1-5** (1672 nm), **1-6** (1860 nm), and **1-8** (2218 nm),[4] is comparable to that of **1-6** (Figure S2, Supporting Information). Therefore, it may be considered that a [26]hexaphyrin unit incorporated to a fused porphyrin tape structure has a large bathochromic-shift-inducing ability that is roughly *as much as that of four fused Zn(II) porphyrin units*.

Cyclic Voltammograms. The electrochemical properties were studied by cyclic voltammetry (CV) and differential pulse voltammetry (DPV) in anhydrous deaerated CH_2Cl_2 (Figure 8 and Figures S32−S38 and Table S2, Supporting Information). The first oxidation and reduction potentials were observed at 0.58 and −1.83 V for Ni(II) porphyrin **21Ni** and 0.36 and −1.93 V for Zn(II) porphyrin **21Zn**, respectively. [26]-Hexaphyrin **3** showed a quasi-reversible oxidation potential at 0.90 V and reversible reduction potentials at −0.57, −0.89, −1.65, and −1.98 V. *meso*−*meso* Singly linked trimer **11** displayed an oxidation potential of the Ni(II) porphyrin segments at 0.62 V and reduction potentials of the [26]-hexaphyrin at −0.70, −1.10, and −1.77 V, and the trimer **17** displayed oxidation potentials of the Zn(II) porphyrin segment at 0.75 and 0.39 V and reduction potentials of the [26]hexaphyrin at −0.70 and −1.04 V. The fact that the first oxidation potentials of the porphyrin segments in **11** and **17** are more positive as compared with those of the reference porphyrin monomers can be interpreted in terms of the electron-withdrawing nature of the [26]hexaphyrin moiety. The observed more negative reduction potentials of the [26]-hexaphyrin in **11** and **17** has been ascribed to a lesser electron-withdrawing nature of the Ni(II) and Zn(II) porphyrin segments as compared with the pentafluorophenyl group. On the basis of these results, the electrochemical HOMO−LUMO gaps were calculated to be 1.32 and 1.09 eV for **11** and **17**, respectively. In contrast, hybrid tape **5** showed an oxidation potential at 0.26 V for the Ni(II) porphyrin and reduction potentials of the [26]hexaphyrin at −0.41, −0.63, −1.08, −1.36, and −1.70 V. The observed negatively and positively shifted oxidation and reduction potentials are thought to be a result of the fused structure, as supported by DFT calculations (Supporting Information). Hybrid tape **6** displayed seven potentials at 0.09, −0.02, −0.54, −0.78, −1.24, −1.47, and −1.88 V all as fully reversible waves. Interestingly, the first oxidation potential of the Zn(II) porphyrins looked split, being observed at 0.09 and −0.02 V with a small energy gap (ΔE = 0.11 V). While the splitting energy is small, this splitting seems to indicate a slight but meaningful electronic interaction between the terminal Zn(II) porphyrins through the long axis of the hexaphyrin moiety. This splitting value of **6** is smaller

DOI: 10.1021/ja5130034
J. Am. Chem. Soc. 2015, 137, 2097−2106

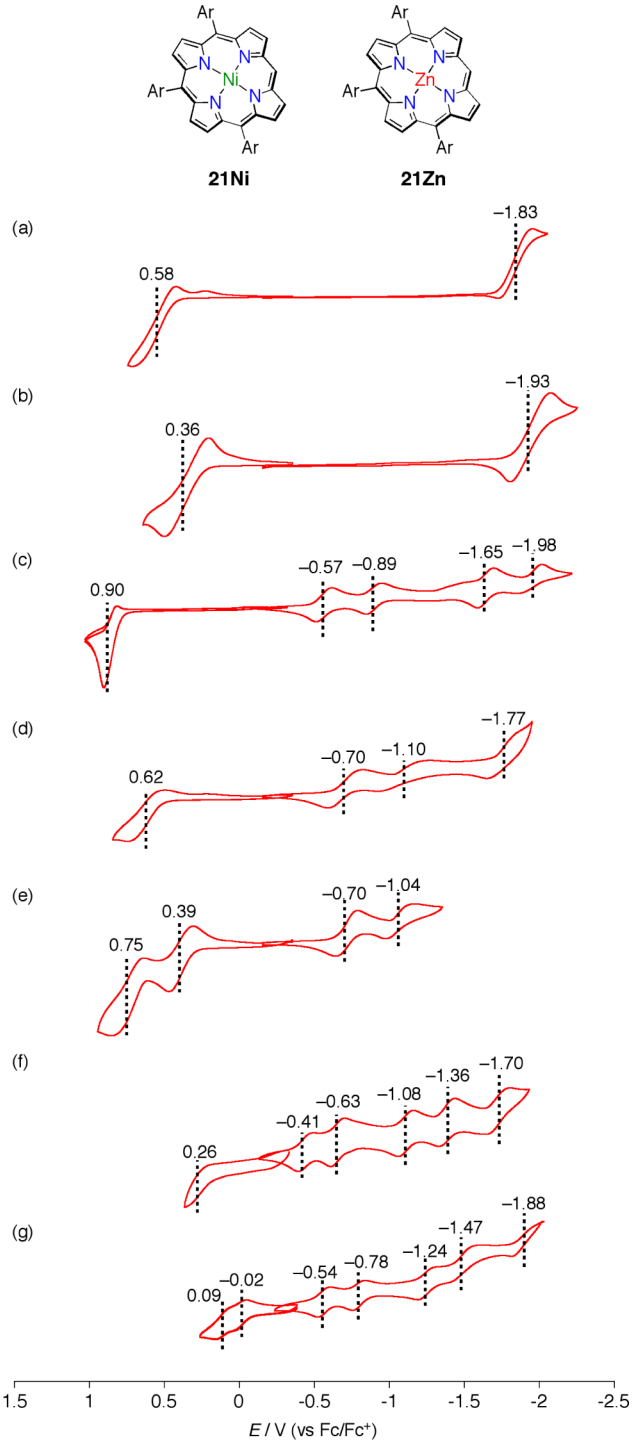

Figure 8. Cyclic voltammograms of (a) **21Ni**, (b) **21Zn**, (c) **3**, (d) **11**, (e) **17**, (f) **5**, and (g) **6** in CH_2Cl_2 versus the ferrocene/ferrocenium ion couple.

than those of previously reported porphyrin tape trimers (ca. 0.17 V).[8a] Another intriguing feature is the five closely spaced reversible reduction waves of **5** and **6**, an attribute that may allow multicharge storage capabilities.[24] Finally, the electrochemical HOMO−LUMO gaps were estimated to be 0.67 and 0.52 eV for **5** and **6**, respectively.

Theoretical Calculations and Excited State Dynamics. Density functional theory (DFT) calculations were performed on the hybrid tapes **5** and **6** with the Gaussian 09 program at the B3LYP/6-31G(d)(C, H, N, F)/LANL2DZ(Ni, Zn) level (Figures S41 and S44, Supporting Information). The calculated orbital diagrams of **5** and **6** are similar to each other. While the LUMO+1 is mostly localized on the hexaphyrin core, the LUMO is effectively spread over the whole molecule through the triply fused structure, indicating strong conjugation. On the other hand, the HOMO−2 is governed by the a_{1u}-like orbital of the terminal porphyrin units, but the HOMO and HOMO−1 are composed of the combination of the a_{2u}- and a_{1u}-like orbitals of the hexaphyrin and porphyrin, again indicating the effective conjugation between each of the chromophores. These calculations are consistent with the oxidation and reduction potentials of **5** and **6** described above.

To examine the excited-state dynamics of *meso*−*meso* linked hybrid arrays and triply linked hybrid tapes, we have measured the femtosecond transient absorption (TA) of compounds **5**, **6**, **11**, **15**, and **17**. For elucidation of the interaction between the [26]hexaphyrin core and porphyrin moieties, we have employed two different excitation wavelengths: 420 nm for excitation of the porphyrin moiety and 700 nm for selective excitation of the [26]hexaphyrin moiety in **11**, **15**, and **17** (Figure 9a and Figure S47, Supporting Information). The TA spectra of these compounds exhibited ground state bleaching signals whose spectral features correspond to their ground-state absorption bands. Although the spectral features of the TA spectra were identical regardless of the excitation wavelength, the decay profiles revealed clear differences. While a fast rise component of approximately a 0.4 ps time constant was observed for λ_{ex} = 420 nm (Figure 9a, inset, and Figure S48, Supporting Information), no such fast rise dynamics was observed and the decay curves were fit with a single exponential function with a time constant of 140 ps in the TA spectra recorded for λ_{ex} = 700 nm. The decays with τ = 140 ps have been ascribed to the excited-state lifetime of the hexaphyrin core, since this time constant is similar to the singlet excited-state lifetime (ca. 100 ps) of [26]hexaphyrin by using the TA technique.[25] The slightly longer lifetimes of **11**, **15**, and **17** likely originate from the attachment of porphyrin moieties at the *meso*-positions. In order to identify the origin of the 0.4 ps dynamics, the time evolution of their transient spectra was globally analyzed (Figure S49, Supporting Information). In the globally analyzed decay-associated spectra, two distinct components were observed with time constants of 0.4 and 140 ps, respectively. Interestingly, the spectral feature of the former resembles that of a porphyrin Q-band, which led us to confirm that the 0.4 ps time component represents the energy transfer rate from the porphyrin to the hexaphyrin moieties. In other words, this result strongly indicates the existence of an efficient excitation energy transfer (EET) process from the porphyrin to the hexaphyrin in **11**, **15**, and **17**. It is worth noting that the EET time constants in **11**, **15**, and **17** showed no significant difference, because the distances between the porphyrin and the hexaphyrin moieties as well as the energy differences between the donor and the acceptor are nearly identical, although each donor porphyrin has a different energy level. The time resolution of our TA setup (~150 fs) also made it almost impossible to differentiate the energy transfer rates between the three compounds. In the case of **11**, we could also observe an additional long time component that might be ascribed to the excited triplet state of the hexaphyrin core. This particular characteristic is unseen in **15** and **17** and most likely comes from the presence of a low-lying metal excited (d,d) state in the Ni(II) porphyrin moieties.[26] The three decay

DOI: 10.1021/ja5130034
J. Am. Chem. Soc. 2015, 137, 2097−2106

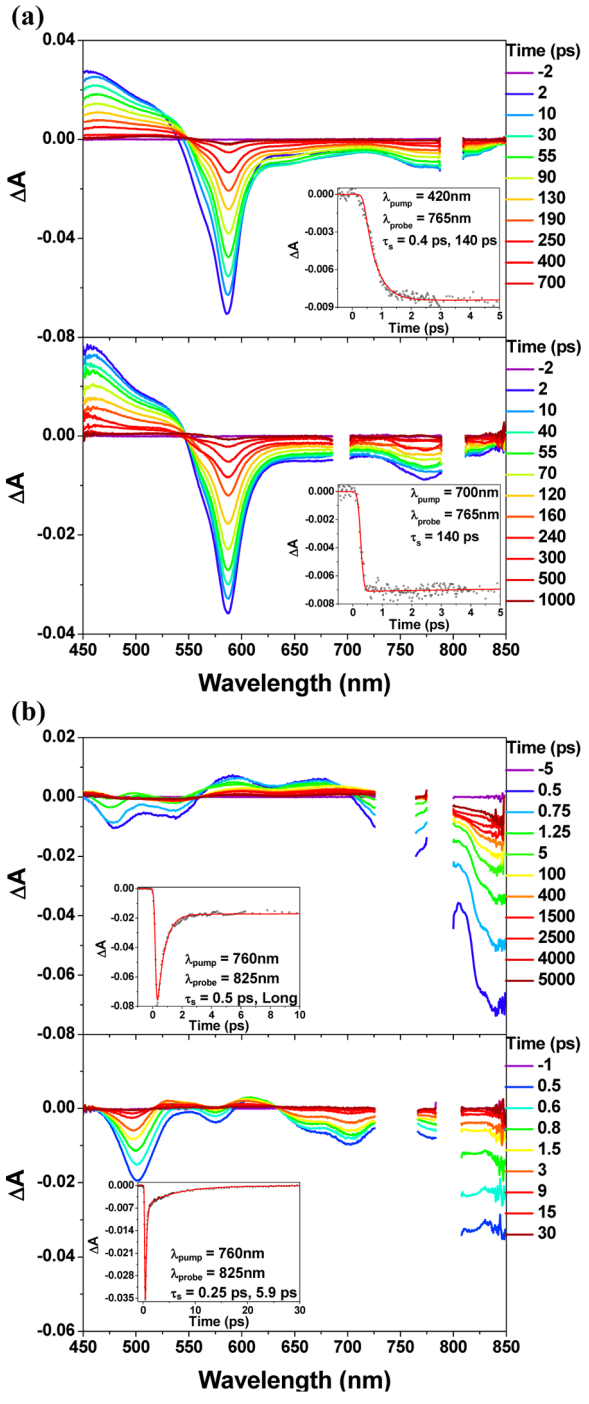

Figure 9. (a) Femtosecond transient absorption spectra of **17** in toluene obtained with photoexcitation at 420 nm (top) and 700 nm (bottom). (b) Femtosecond transient absorption spectra of **5** (top) and **6** (bottom) in toluene obtained with photoexcitation at 760 nm. The decay profiles are presented in each TA spectrum.

components observed for **11** can be explained by assuming the photoexcitation of the hybrid array followed by a transition to the (d,d) state and subsequent interaction with the excited triplet state of the adjacent hexaphyrin core. The possible contribution of photoexcitation of the Ni(II) porphyrin moiety to the formation of the excited triplet state of the hexaphyrin core is further suggested by the fact that the amplitude of the long residual upon photoexcitation at 420 nm is larger than that at 720 nm.

In contrast with the *meso*−*meso* singly linked hybrid systems, we could not observe fast rise dynamics at any excitation wavelength in the hybrid tapes **5** and **6**. Instead, ultrafast decay components of 0.5 (**5**) and 0.25 (**6**) ps were observed in addition to a long residual one in **5** and a longer time component of 5.9 ps in **6** (Figure 9b and Figure S50, Supporting Information). Compared to *meso*−*meso* linked hybrids **11** and **17**, the hybrid tapes **5** and **6** exhibit significantly shorter excited-state decay dynamics because of the unified and thus expanded π-conjugation network that causes a reduced energy gap between the excited state and the ground state. However, the trends of the decay components observed in **5** and **6** are notably different from each other. The excited-state dynamics of the hybrid tape **6** are similar to those (0.3 and 5 ps) of hexameric Zn(II) porphyrin tape **1-6** with a similar S_1−S_0 energy gap (0.67 eV).[27] In contrast, the hybrid tape **5** displays a long residual component of > ∼5 ns, which has been attributed to the excited triplet state of the hexaphyrin core by referring to the decay dynamics of **11**. Meanwhile, we conjecture that the 0.5 ps component originates from a combination of the two different contributions, i.e., the transition from the (d,d) state of the peripheral Ni(II) porphyrin moieties to the triplet excited state of the hexaphyrin core and the relaxation of the singlet excited state of Ni(II) porphyrin to its (d,d) state. Such an interpretation by considering a low-lying (d,d) state or the triplet excited state of the hexaphyrin cannot be applied to the excited-state dynamics of **6**, since the Zn(II) porphyrin is devoid of a low-lying (d,d) state. This is probably why we could not observe any long residual components in the decay dynamics of **6**. In general, it is expected that a lifetime of an excited state with a small S_1−S_0 energy gap is largely governed by a small S_1−S_0 energy gap. In such cases, two different relaxation processes are important in determining their decays; one is an electronic transition, and the other is intramolecular and intermolecular vibrational relaxation processes.[28] Importantly, the 5.9 ps decay component observed for **6** is longer than that (4.5 ps) in Zn(II) dimeric tape **1-2**[27] despite the smaller energy gap. This finding may indicate that the excited-state dynamics of **6** cannot be fully explained in terms of the energy gap law. In π-conjugated fused molecular arrays such as **6**, the energy level of the S1 state can be significantly lowered, eventually becoming comparable to those of vibrational energy states. In such molecules, the competition between the above two relaxation processes plays an important role in the excited-state dynamics, which leads us to assume that the contribution from vibrational relaxation processes cannot be neglected. Therefore, the 5.9 ps decay component observed for **6** has been attributed to vibrational relaxation processes. Consequently, we assume that the decay time component of 0.5 ps and long residual one in the decay of **5** are attributed to the (d,d) state of Ni(II) porphyrin moieties and the formation of the triplet state of the hexaphyrin core, and the 0.25 ps decay component of **6** is thus attributed to the electronic relaxation process.

CONCLUSIONS

meso−*meso* Singly linked Ni(II) porphyrin−[26]hexaphyrin−Ni(II) porphyrin hybrid trimers **9** and **11** were prepared by the cross-condensation of *meso*-formyl Ni(II) porphyrins **7** or **10** with tripyrrane **8**, respectively. The Ni(II) ions in the porphyrins were changed to Zn(II) ions via an indirect route involving reduction to the [28]hexaphyrin congeners, denickelation, and Zn(II) metal insertion to furnish the corresponding

DOI: 10.1021/ja5130034
J. Am. Chem. Soc. 2015, 137, 2097−2106

trimers **16** and **17**. Over the course of these transformations, porphyrin−[28]hexaphyrin−porphyrin trimers have been revealed to adopt a Möbius aromatic twisted structure for the [28]hexaphyrin moiety in solution despite the presence of two directly linked porphyrin segments. The oxidative *meso*−*meso* coupling reactions of **16** produced the corresponding dimer, trimer, and tetramer. The oxidative fusion reactions of **11** and **17** gave porphyrin−[26]hexaphyrin hybrid tapes **5** and **6**, which showed remarkably red-shifted Q-bands, six and seven reversible redox potentials, and narrow HOMO−LUMO band gaps. It has been demonstrated that when a [26]-hexaphyrin core is incorporated into a hybrid porphyrin tape it displays remarkable bathochromic-shifting abilities, almost equivalent to the inclusion of a Zn(II) porphyrin tetramer. Hence, this work demonstrates that the fusion of porphyrins to a [26]hexaphyrin core offers an efficient means of expanding their conjugation networks, significantly broadening the optical and electronic properties attainable for these chromophores.

■ ASSOCIATED CONTENT

Ⓢ Supporting Information

Preparation and analytical data for samples, detailed crystallographic data for **6**, **9**, **11**, **12**, and **16** (CIF), cyclic voltammograms, calculated molecular orbitals, time-resolved fluorescence decays, and nanosecond time-resolved transient absorption decays. This material is available free of charge via the Internet at http://pubs.acs.org.

■ AUTHOR INFORMATION

Corresponding Authors

*dongho@yonsei.ac.kr

*osuka@kuchem.kyoto-u.ac.jp

Notes

The authors declare no competing financial interest.

■ ACKNOWLEDGMENTS

The work at Kyoto was supported by JSPS KAKENHI Grant Nos. 25220802 and 25620031. H.M. acknowledges JSPS Fellowship for Young Scientists. The work at Yonsei was supported by the Global Research Laboratory (GRL) Program (2013-8-1472) of the Ministry of Education, Science, and Technology (MEST) of Korea. We thank Prof. H. Shinokubo and Dr. S. Hiroto at Nagoya University for X-ray diffraction analysis of **6** and Prof. Dr. H. Maeda and Dr. Y. Bando at Ritsumeikan University for MALDI-TOF MS measurement.

■ REFERENCES

(1) (a) Vicente, M. G. H.; Jaquinod, L.; Smith, K. M. *Chem. Commun.* **1999**, 1771−1782. (b) Anderson, H. L. *Chem. Commun.* **1999**, 2323−2330. (c) Arnold, D. P. *Synlett* **2000**, 296−305. (d) Holten, D.; Bocian, D. F.; Lindsey, J. S. *Acc. Chem. Res.* **2002**, *35*, 57−69. (d) Senge, M. O.; Fazekas, M.; Notaras, E. G. A.; Blau, W. J.; Zawadzka, M.; Locos, O. B.; Mhuircheartaigh, E. M. N. *Adv. Mater.* **2007**, *19*, 2737−2774. (e) Pawlicki, M.; Collins, H. A.; Denning, R. G.; Anderson, H. L. *Angew. Chem., Int. Ed.* **2009**, *48*, 3244−3266. (f) Davis, N. K. S.; Thompson, A. L.; Anderson, H. L. *J. Am. Chem. Soc.* **2011**, *133*, 30−31. (g) Lewtak, J. P.; Gryko, D. T. *Chem. Commun.* **2012**, *48*, 10069−10086.

(2) (a) Crossley, M. J.; Burn, P. L. *J. Chem. Soc., Chem. Commun.* **1991**, 1569−1571. (b) Arnold, D. P.; Heath, G. A. *J. Am. Chem. Soc.* **1993**, *115*, 12197−12198. (c) Lin, V. S.-Y.; DiMagno, S. G.; Therien, M. J. *Science* **1994**, *264*, 1105−1111. (d) Jaquinod, L.; Siri, O.; Khoury, R. G.; Smith, K. M. *Chem. Commun.* **1998**, 1261−1262. (e) Hoffmann, M.; Wilson, C. J.; Odell, B.; Anderson, H. L. *Angew. Chem., Int. Ed.* **2007**, *46*, 3122−3125.

(3) (a) Kim, D.; Osuka, A. *Acc. Chem. Res.* **2004**, *37*, 735−745. (b) Aratani, N.; Kim, D.; Osuka, A. *Chem.—Asian J.* **2009**, *4*, 1172−1182. (c) Mori, H.; Tanaka, T.; Osuka, A. *J. Mater. Chem. C* **2013**, *1*, 2500−2519. (d) Tanaka, T.; Osuka, A. *Chem. Soc. Rev.* **2015**, DOI: 10.1039/C3CS60443H.

(4) Tsuda, A.; Osuka, A. *Science* **2001**, *293*, 79−82.

(5) (a) Tsuda, A.; Nakano, A.; Furuta, H.; Yamochi, H.; Osuka, A. *Angew. Chem., Int. Ed.* **2000**, *39*, 558−561. (b) Tsuda, A.; Furuta, H.; Osuka, A. *Angew. Chem., Int. Ed.* **2000**, *39*, 2549−2552. (c) Tsuda, A.; Furuta, H.; Osuka, A. *J. Am. Chem. Soc.* **2001**, *123*, 10304−10321.

(6) (a) Ahn, T. K.; Kim, K. S.; Kim, D. Y.; Noh, S. B.; Aratani, N.; Ikeda, C.; Osuka, A.; Kim, D. *J. Am. Chem. Soc.* **2006**, *128*, 1700−1704. (b) Yoon, M.-C.; Noh, S. B.; Tsuda, A.; Nakamura, Y.; Osuka, A.; Kim, D. *J. Am. Chem. Soc.* **2007**, *129*, 10080−10081.

(7) (a) Nakamura, Y.; Jang, S. Y.; Tanaka, T.; Aratani, N.; Lim, J. M.; Kim, K. S.; Kim, D.; Osuka, A. *Chem.—Eur. J.* **2008**, *14*, 8279−8289. (b) Nakamura, Y.; Aratani, N.; Shinokubo, H.; Takagi, A.; Kawai, T.; Matsumoto, T.; Yoon, Z. S.; Kim, D. Y.; Ahn, T. K.; Kim, D.; Muranaka, A.; Kobayashi, N.; Osuka, A. *J. Am. Chem. Soc.* **2006**, *128*, 4119−4127.

(8) (a) Tanaka, T.; Lee, B. S.; Aratani, N.; Yoon, M.-C.; Kim, D.; Osuka, A. *Chem.—Eur. J.* **2011**, *17*, 14400−14412. (b) Mori, H.; Tanaka, T.; Lee, B. S.; Kim, P.; Kim, D.; Osuka, A. *Chem.—Asian J.* **2012**, *7*, 1811−1816.

(9) Bonifazi, D.; Scholl, M.; Song, F. Y.; Echegoyen, L.; Accorsi, G.; Armaroli, N.; Diederich, F. *Angew. Chem., Int. Ed.* **2003**, *42*, 4966−4970.

(10) Sato, H.; Tashiro, K.; Shinmori, H.; Osuka, A.; Murata, Y.; Komatsu, K.; Aida, T. *J. Am. Chem. Soc.* **2005**, *127*, 13086−13087.

(11) Sakurai, T.; Shi, K.; Sato, H.; Tashiro, K.; Osuka, A.; Saeki, A.; Seki, S.; Tagawa, S.; Sasaki, S.; Matsunaga, H.; Osaka, K.; Tasaka, M.; Aida, T. *J. Am. Chem. Soc.* **2008**, *130*, 13812−13813.

(12) (a) Neves, M. G. P. M. S.; Martins, R. M.; Tomé, A. C.; Silvestre, A. J. D.; Silva, A. M. S.; Félix, V.; Drew, M. G. B.; Cavaleiro, J. A. S. *Chem. Commun.* **1999**, 385−386. (b) Shin, J.-Y.; Furuta, H.; Yoza, K.; Igarashi, S.; Osuka, A. *J. Am. Chem. Soc.* **2001**, *123*, 7190−7191.

(13) (a) Tanaka, T.; Aratani, N.; Lim, J. M.; Kim, K. S.; Kim, D.; Osuka, A. *Chem. Sci.* **2011**, *2*, 1414−1418. (b) Tanaka, T.; Aratani, N.; Osuka, A. *Chem.—Asian J.* **2012**, *7*, 889−893.

(14) Taniguchi, R.; Shimizu, S.; Suzuki, M.; Shin, J.-Y.; Furuta, H.; Osuka, A. *Tetrahedron Lett.* **2003**, *44*, 2505−2507.

(15) Crystallographic data for **9**: monoclinic, space group $P2_1/n$ (no. 14), a = 16.3245(3), b = 25.3066(5), c = 20.3499(4) Å, β = 97.9906(7)°, V = 8325.3(3) Å^3, T = 93 K, Z = 2, R_1 = 0.0818 ($I > 2\sigma(I)$), R_w = 0.2589 (all data), GOF = 1.025. CCDC number: 1036490.

(16) Crystallographic data for **11**: triclinic, space group P-1 (no. 2), a = 14.4663(14), b = 20.885(2), c = 22.059(2) Å, α = 77.33(2), β = 75.06(3), γ = 71.62(3)°, V = 6041.2(10) Å^3, T = 93 K, Z = 1, R_1 = 0.1076 ($I > 2\sigma(I)$), R_w = 0.3430 (all data), GOF = 1.002. CCDC number: 1036493. The contributions to the scattering arising from the presence of the disordered solvents in the crystal were removed by use of the utility SQUEEZE in the PLATON software package.

(17) Sankar, J.; Mori, S.; Saito, S.; Rath, H.; Suzuki, M.; Inokuma, Y.; Shinokubo, H.; Kim, K. S.; Yoon, Z. S.; Shin, J.-Y.; Lim, J. M.; Matsuzaki, Y.; Matsushita, O.; Muranaka, A.; Kobayashi, N.; Kim, D.; Osuka, A. *J. Am. Chem. Soc.* **2008**, *130*, 13568−13579.

(18) Crystallographic data for **12**: triclinic, space group P-1 (no. 2), a = 14.6906(3), b = 19.7967(4), c = 28.3889(7) Å, α = 78.8254(13), β = 78.9164(11), γ = 75.3523(12)°, V = 8325.3(3) Å^3, T = 93 K, Z = 2, R_1 = 0.1280 ($I > 2\sigma(I)$), R_w = 0.3748 (all data), GOF = 1.080. CCDC number: 1036491.

(19) Mori, S.; Shimizu, S.; Shin, J.-Y.; Osuka, A. *Inorg. Chem.* **2007**, *46*, 4374−4376.

(20) (a) Osuka, A.; Shimidzu, H. *Angew. Chem., Int. Ed. Engl.* **1997**, *36*, 135−137. (b) Yoshida, N.; Shimidzu, H.; Osuka, A. *Chem. Lett.* **1998**, 55−56.

DOI: 10.1021/ja5130034
J. Am. Chem. Soc. 2015, 137, 2097−2106

(21) (a) Jin, L.-M.; Chen, L.; Yin, J.-J.; Guo, C.-C.; Chen, Q.-Y. *Eur. J. Org. Chem.* **2005**, 3994−4001. (b) Jin, L.-M.; Yin, J.-J.; Chen, L.; Guo, C.-C.; Chen, Q.-Y. *Synlett* **2005**, 2893−2898. (c) Ouyang, Q.; Zhu, Y.-Z.; Zhang, C.-H.; Yan, K.-O.; Li, Y.-C.; Zheng, J. Y. *Org. Lett.* **2009**, *11*, 5266−5269.

(22) Kamo, M.; Tsuda, A.; Nakamura, Y.; Aratani, N.; Furukawa, K.; Kato, T.; Osuka, A. *Org. Lett.* **2003**, *5*, 2079−2082.

(23) Crystallographic data for **6**: $C_{178}H_{148}N_{14}F_{20}Zn_2\cdot(MeOH)_2$, triclinic, space group *P*-1 (no. 2), a = 13.4503(13), b = 19.9780(12), c = 20.980(2) Å, α = 70.61(2), β = 74.74(2), γ = 74.356(17)°, V = 5026.3(7) Å^3, T = 123 K, Z = 1, R_1 = 0.0837 ($I > 2\sigma(I)$), R_w = 0.2580 (all data), GOF = 1.035. CCDC number: 1036494. The contributions to the scattering arising from the presence of the disordered solvents in the crystal were removed by use of the utility SQUEEZE in the PLATON software package.

(24) Naoda, K.; Mori, H.; Aratani, N.; Lee, B. S.; Kim, D.; Osuka, A. *Angew. Chem., Int. Ed.* **2012**, *51*, 9856−9859.

(25) Cha, W.-Y.; Lim, J. M.; Yoon, M.-C.; Sung, Y. M.; Lee, B. S.; Katsumata, S.; Suzuki, M.; Mori, H.; Ikawa, Y.; Furuta, H.; Osuka, A.; Kim, D. *Chem.—Eur. J.* **2012**, *18*, 15838−15844.

(26) Eom, H. S.; Jeoung, S. C.; Kim, D.; Ha, J.-H.; Kim, Y. R. *J. Phys. Chem. A* **1997**, *101*, 3661−3669.

(27) Cho, H. S.; Jeong, D. H.; Cho, S.; Kim, D.; Matsuzaki, Y.; Tanaka, K.; Tsuda, A.; Osuka, A. *J. Am. Chem. Soc.* **2002**, *124*, 14642−14654.

(28) Kim, P.; Ikeda, T.; Lim, J. M.; Park, J.; Lim, H.; Aratani, N.; Osuka, A.; Kim, D. *Chem. Commun.* **2011**, *47*, 4433−4435.

DOI: 10.1021/ja5130034
J. Am. Chem. Soc. 2015, 137, 2097−2106